nature biotechnology

Differentiation of pluripotent stem cells to muscle fiber to model Duchenne muscular dystrophy

Jérome Chal[1–5], Masayuki Oginuma[1], Ziad Al Tanoury[1], Bénédicte Gobert[1], Olga Sumara[1], Aurore Hick[6], Fanny Bousson[6], Yasmine Zidouni[1], Caroline Mursch[1], Philippe Moncuquet[1], Olivier Tassy[1], Stéphane Vincent[1], Ayako Miyanari[1], Agata Bera[1], Jean-Marie Garnier[1], Getzabel Guevara[3–5], Marie Hestin[3–5], Leif Kennedy[1], Shinichiro Hayashi[7,8], Bernadette Drayton[7,8], Thomas Cherrier[1], Barbara Gayraud-Morel[9], Emanuela Gussoni[10], Frédéric Relaix[7,8], Shahragim Tajbakhsh[9] & Olivier Pourquié[1–5,11]

During embryonic development, skeletal muscles arise from somites, which derive from the presomitic mesoderm (PSM). Using PSM development as a guide, we establish conditions for the differentiation of monolayer cultures of mouse embryonic stem (ES) cells into PSM-like cells without the introduction of transgenes or cell sorting. We show that primary and secondary skeletal myogenesis can be recapitulated *in vitro* from the PSM-like cells, providing an efficient, serum-free protocol for the generation of striated, contractile fibers from mouse and human pluripotent cells. The mouse ES cells also differentiate into Pax7$^+$ cells with satellite cell characteristics, including the ability to form dystrophin$^+$ fibers when grafted into muscles of dystrophin-deficient *mdx* mice, a model of Duchenne muscular dystrophy (DMD). Fibers derived from ES cells of *mdx* mice exhibit an abnormal branched phenotype resembling that described *in vivo*, thus providing an attractive model to study the origin of the pathological defects associated with DMD.

© 2015 Nature America, Inc. All rights reserved.

Skeletal muscles constitute the most abundant tissue in the human body. Several degenerative diseases of the muscle, such as DMD, may be treatable with cell therapy approaches if healthy muscle progenitors could be grafted in patients to recreate lost muscles and resident stem cells[1]. Efficient generation of functional muscle cells *in vitro* from pluripotent cells has so far been achieved only by introducing exogenous DNA into the cells to force expression of transcription factors such as Myod1, Pax3 and Pax7 (refs. 2–7). Embryoid bodies generated from mouse ES cells in various conditions can differentiate into a wide range of cell types derived from the three germ layers, including skeletal muscle[8–10]. However, this strategy allows poor control and reproducibility of the differentiation process and usually yields mixed populations with low percentages of the target cell population. In several recent studies using embryoid bodies to produce skeletal muscle from mouse or human pluripotent cells, neither the differentiation efficiency nor the degree of differentiation has been documented[11–16]. An alternative approach—differentiation of pluripotent cells in monolayers by modulation of signaling pathways to induce a paraxial mesoderm fate[17–24]—has led mostly to limited production of paraxial mesoderm precursors, necessitating enrichment by cell sorting. Furthermore, these studies have not shown production of contractile millimeter-size fibers with organized myofibrils and their associated satellite muscle stem cells in their niche.

Here we recapitulate the development of the muscle lineage *in vitro* from mouse and human pluripotent stem cells to produce multinucleated muscle fibers with organized myofibrils and Pax7$^+$ cells exhibiting characteristics of satellite cells. The Pax7$^+$ cells are able to reconstitute muscle fibers and satellite cells when grafted into the muscle of *mdx* mice, which lack dystrophin, the protein mutated in DMD. *mdx* muscle fibers differentiated from ES cells *in vitro* show a striking increase in the number of branches, reminiscent of that observed in individuals with DMD.

RESULTS

Transcriptome landscape during PSM differentiation

We first set out to recapitulate the early stages of differentiation of the myogenic lineage in the PSM. The posterior-to-anterior maturation gradient of the PSM means that within a single embryo the different stages of differentiation are spatially mapped out along the posterior-to-anterior axis. We therefore profiled the full process of differentiation from the tail bud stage to the onset of myogenesis by microarray analysis of consecutive fragments stretching from the tail bud to the newly formed somite of embryonic day (E)9.5 mouse embryos (**Fig. 1a**,**b** and **Supplementary Fig. 1**). The resulting representation of gene expression along the PSM during early stages of paraxial mesoderm differentiation was consistent with data from *in situ* hybridization, as exemplified by

[1]Institut de Génétique et de Biologie Moléculaire et Cellulaire (IGBMC), CNRS (UMR 7104), Inserm U964, Université de Strasbourg, Illkirch Graffenstaden, France. [2]Stowers Institute for Medical Research, Kansas City, Missouri, USA. [3]Department of Pathology, Brigham and Women's Hospital, Boston, Massachusetts, USA. [4]Department of Genetics, Harvard Medical School, Boston, Massachusetts, USA. [5]Harvard Stem Cell Institute, Boston, Massachusetts, USA. [6]Anagenesis Biotechnologies, Parc d'innovation, Illkirch Graffenstaden, France. [7]UPMC Paris 06, UMRS 787, INSERM, Avenir team, Pitié-Salpêtrière, Paris, France. [8]Institut de Myologie, Paris, France. [9]Institut Pasteur, CNRS URA 2578, Paris, France. [10]Division of Genetics and Genomics Boston Children's Hospital, Boston, Massachusetts, USA. [11]Howard Hughes Medical Institute, Kansas City, Missouri, USA. Correspondence should be addressed to O.P. (pourquie@genetics.med.harvard.edu).

Received 9 February; accepted 23 June; published online 3 August 2015; doi:10.1038/nbt.3297

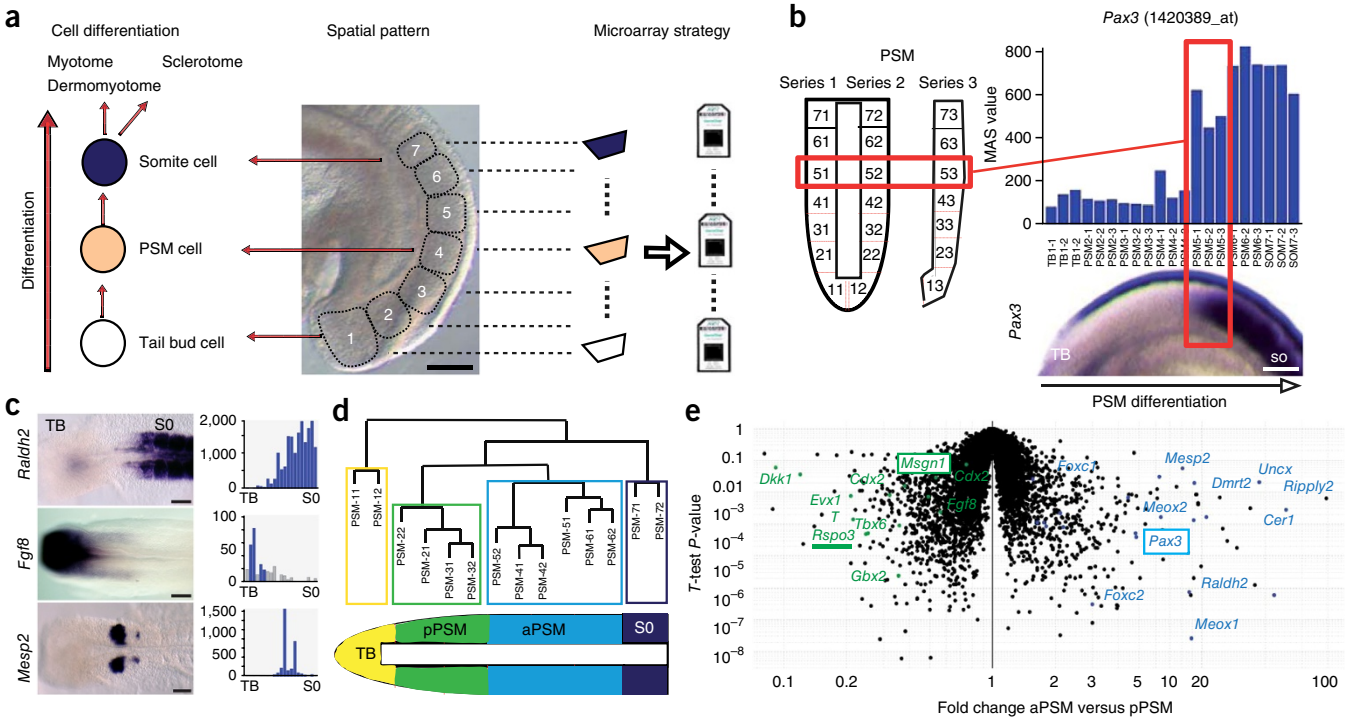

Figure 1 Molecular profiling of early stages of paraxial mesoderm differentiation. (**a**) Strategy used to produce the microarray series of early paraxial mesoderm differentiation stages. Middle panel shows the left side of the posterior part of an E9.5 mouse embryo indicating the location of the dissected fragments used to generate the microarrays. Tissue fragments were numbered 1 to 7, along the posterior to anterior axis, starting from the tail bud domain (1), then 5 consecutive fragments of the PSM and the forming somite (7). Scale bar, 100 µm. (**b**) The generation of gene expression histograms from the microarray series. (Left) The 3 series of microdissected PSM fragments used for microarray generation. (Right) Histogram showing *Pax3* expression dynamics during PSM differentiation. Red boxes indicate the correspondence between the microdissected samples series, the expression profile histogram (blue bars) and the corresponding transcript expression in the right PSM detected by *in situ* hybridization (bottom). A single probe set corresponding to *Pax3* is shown. The histogram was generated from MicroArray Suite (MAS) expression value for a given probe set, with samples of the three microdissection series arranged according to their position along the antero-posterior axis (posterior to the left). The resulting profile gives a quantitative view of transcript expression during early stages of paraxial mesoderm differentiation. TB, Tail bud; S0, last formed somite. Scale bar, 100 µm. (**c**) Microarray data validation. Comparison of the PSM expression of the genes *Raldh2*, *Fgf8* and *Mesp2* detected by *in situ* hybridization (left) in E8.5 mouse embryos (dorsal view, posterior to the left) with their expression profile in the microarray series; blue histograms show the expression levels of a probe set (as described in **b**), corresponding to the genes shown on the left. Scale bars, 100 µm. (**d**) Hierarchical clustering of the microarrays of the paraxial mesoderm series. Clusters with $P > 0.95$ are highlighted by color-coded boxes which identify four major transcriptional domains corresponding to TB (yellow), posterior PSM (pPSM, green), anterior PSM (aPSM, blue) and somite (SO, dark blue). For the aPSM, only the two subclusters exhibit $P > 0.95$. (**e**) Volcano scatter plot comparing aPSM versus pPSM microarray expression data sets. Each domain expression profile was obtained by averaging the corresponding clustered arrays (**Fig. 1d**). The ratio of expression for each probe set is plotted on *x* axis (fold change, logarithmic scale); its significance on the *y* axis (*t*-test *P* value, logarithmic scale). Total probe sets shown are about 45,000 from which about 15,000 are considered significant ($P < 0.05$). Well-characterized signature genes enriched in the pPSM (in green) and in the aPSM (in blue) are shown. Note that *Rspo3* (underlined, in green) is significantly upregulated in the pPSM.

well-characterized genes such as the fibroblast growth factor (FGF) ligand *Fgf8* and the retinoic acid biosynthetic enzyme *Raldh2* (also known as *Aldh1a2*), which show anterior or posterior graded expression in the PSM, and by *Mesp2*, which shows a striped expression (**Fig. 1c**).

Clustering analysis revealed that the mouse PSM can be subdivided into anterior and posterior transcriptional domains (**Fig. 1d**), as previously reported for zebrafish[25]. A comparison of gene expression fold changes between the two domains (**Fig. 1e**) identified 285 genes upregulated in the anterior PSM and 330 in the posterior PSM with a fold change >2 ($P < 0.05$). These included most genes known to be specific for either anterior or posterior PSM, such as *Msgn1* and *Pax3*, respectively (**Fig. 1e** and **Supplementary Table 1**).

Wnt activation and BMP inhibition lead to a PSM fate

We reasoned that a successful myogenic differentiation protocol might have to mimic these important transitions of the developing PSM. To monitor the differentiation of ES cells toward the posterior PSM fate, we generated a transgenic mouse ES cell line (Msgn1-repV for *Mesogenin1* reporter Venus) in which the promoter of the posterior PSM–specific gene *Msgn1* (ref. 26) drives expression of Venus fluorescent protein. Embryos generated by tetraploid aggregation from Msgn1-repV cells faithfully expressed the reporter in the posterior PSM (**Fig. 2a**). To identify secreted factors able to guide differentiation of ES cells toward the posterior PSM fate, we searched the microarray series for secreted factors specifically expressed in this domain. One such factor showing strong enrichment in the posterior PSM was the Wnt activator R-spondin3 (*Rspo3*)[27] (**Fig. 1e** and **Supplementary Table 1**). By *in situ* hybridization, *Rspo3* exhibited a graded expression specific to the posterior PSM (**Fig. 2b**). When monolayers of Msgn1-repV cells were cultured in serum-free medium supplemented with Rspo3 and the Bmp inhibitor LDN193189 ('RDL' medium, to block lateral plate mesoderm induction[28]), large numbers (45–65%) of Venus$^+$ (M$^+$) cells were observed after 4 d of differentiation (**Fig. 2c**). M$^+$ cells generated in RDL medium showed strong upregulation of

© 2015 Nature America, Inc. All rights reserved.

the paraxial mesoderm markers *Tbx6*, *Hes7* and *Msgn1*, and very low levels of the lateral plate marker *Foxf1a* (also known as *Foxf1*) and of the cardiac marker *Nkx2-5* (**Fig. 2d**). At day 4, a majority of the M$^+$ cells also expressed the PSM-marker Tbx6 (**Fig. 2g**).

We next compared the transcriptional identity of the M$^+$ cells cultured in serum-free RDL medium for 4 d to their *in vivo* counterparts, the posterior PSM cells (**Figs. 1d** and **2i**). During differentiation from ES cells, M$^+$ cells upregulated a large number of posterior PSM signature genes, including *Msgn1*, *Tbx6*, *Dkk1*, *Rspo3*, *Cdx2* and *Evx1* as observed *in vivo* (**Fig. 2i** and **Supplementary Table 2**). Thus, *in vitro* differentiation of the Msgn1-repV reporter ES cells in the presence of Rspo3 and a BMP inhibitor efficiently induced their differentiation toward

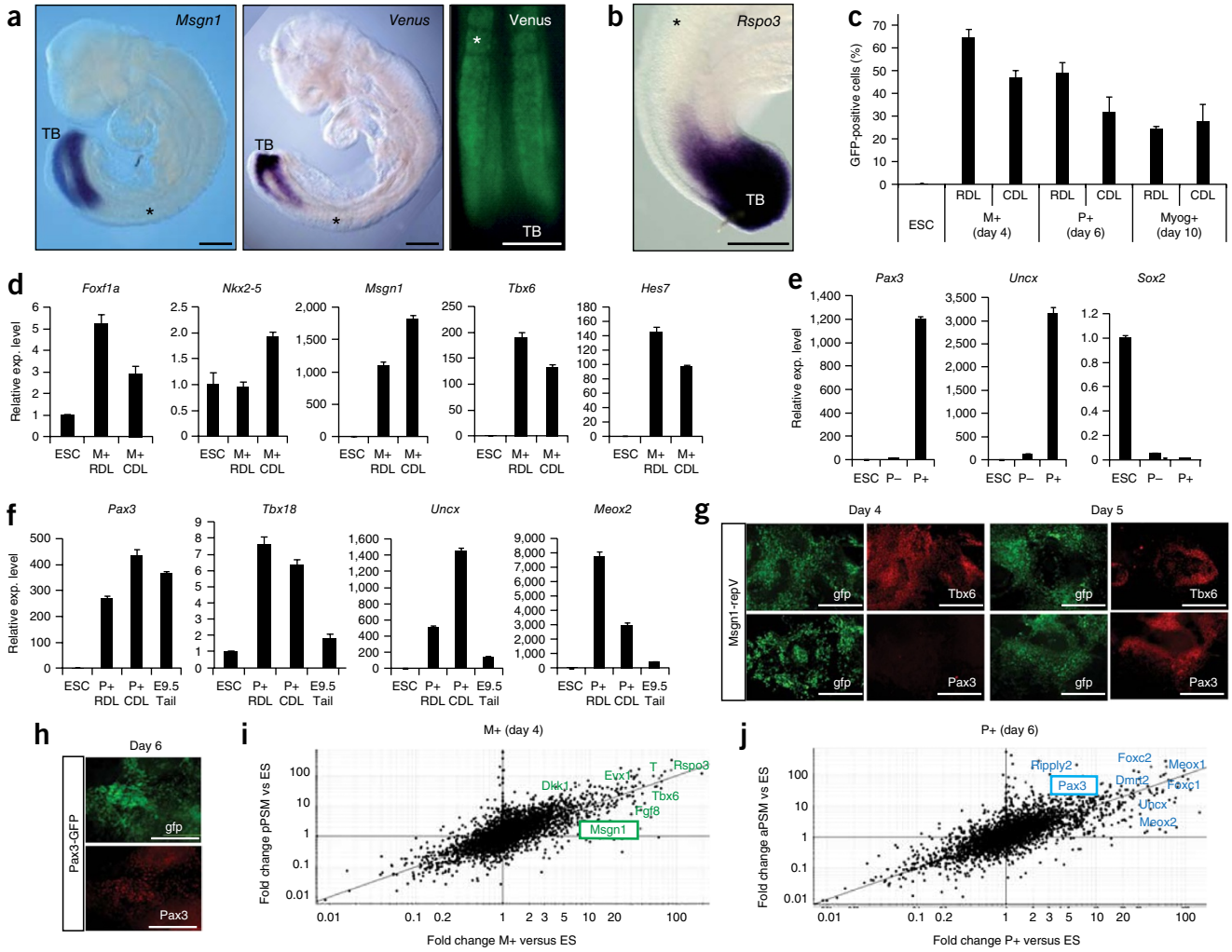

Figure 2 *In vitro* differentiation of ES cells toward a PSM-like fate. (**a**) (Left) E9.0 mouse embryo hybridized with *Msgn1*, showing transcript expression restricted to the pPSM. (Right) Mouse E9.0 embryos derived from Msgn1-repV ES cells by tetraploid aggregation. *In situ* hybridization showing that *Venus* expression is restricted to the pPSM (left); the more stable protein is detected in the PSM and newly formed somites (right, dorsal view, anterior to the top). *, the level of the newly formed somite. TB, tail bud. Scale bars, 200 µm. (**b**) Expression of *Rspo3* mRNA detected by *in situ* hybridization in an E9.5 mouse embryo. Asterisk, newly formed somite. Lateral view, anterior to the top. Scale bar, 200 µm. (**c**) Induction of Msgn1-repV$^+$ (M$^+$), Pax3-GFP$^+$ (P$^+$) and Myog-repV$^+$ cells after, respectively, 4, 6 and 10 d of differentiation in Rspo3 (RDL) or Chir (CDL) serum-free media. Error bars, mean ± s.d. (**d**) qRT-PCR analysis of the lateral plate marker *Foxf1a*, the cardiac marker *Nkx2-5* and the PSM markers *Msgn1*, *Tbx6* and *Hes7* on FACS-sorted Msgn1-repV$^+$ (M$^+$) cells after 4 d in Rspo3 (RDL) or Chir (CDL) serum-free media. ES cells (ESC) expression data are normalized to 1. Error bars, mean ± s.d. (**e**) qRT-PCR analysis comparing the expression level of *Pax3*, *Uncx* and *Sox2* in undifferentiated ESCs, and in FACS-sorted Pax3-GFP$^+$ (P$^+$) and Pax3-GFP$^-$ (P$^-$) cells differentiated for 6 d in serum-free RDL medium. P$^-$ expression data are normalized to 1. Error bars, mean ± s.d. P$^+$ cell fraction expresses significantly higher level of *Pax3* and *Uncx* and lower level of *Sox2* when compared to P$^-$ or ES cell fractions ($P < 0.0005$). (**f**) qRT-PCR analysis comparing the expression level of the aPSM markers *Pax3*, *Tbx18*, *Uncx* and *Meox2* in mouse ESCs, and in FACS-sorted Pax3-GFP$^+$ (P$^+$) cells after 6 d of differentiation in RDL or CDL medium, and with E9.5 mouse PSM tail. ESC data are normalized to 1. Error bars, mean ± s.d. (**g**) Comparison of GFP and Tbx6 or Pax3 proteins expression in culture of Msgn1-repV reporter cells differentiated in RDL medium for days 4 and 5. Scale bars, 400 µm. (**h**) Comparison of GFP and Pax3 proteins in culture of Pax3-GFP reporter cells differentiated in RDL medium for 6 d. Scale bars, 200 µm. (**i**) Fold change versus fold change (FcFc) scatter plot comparing FACS-sorted M$^+$ cells differentiated for 4 d in RDL medium to ESCs and pPSM microarrays to ESCs microarray expression data sets. The ratio of expression for each probe set and for each comparison is plotted on *x* axis and *y* axis, respectively (fold change, logarithmic scale). Probe sets (about 3,400) with a *t*-test $P < 0.05$ (**Fig. 1e**) are shown. Green, known signature genes specific for the pPSM. (**j**) FcFc scatter plot comparing FACS-sorted P$^+$ cells differentiated for 6 d in RDL medium to ES cells and aPSM microarrays to ESC microarray expression data sets. The ratio of expression for each probe sets for each comparison is plotted on *x* axis and *y* axis, respectively (fold change, logarithmic scale). Probe sets (about 3,400) with a *t*-test $P < 0.05$ (**Fig. 1e**) are shown. Blue, known signature genes specific for the aPSM.

© 2015 Nature America, Inc. All rights reserved.

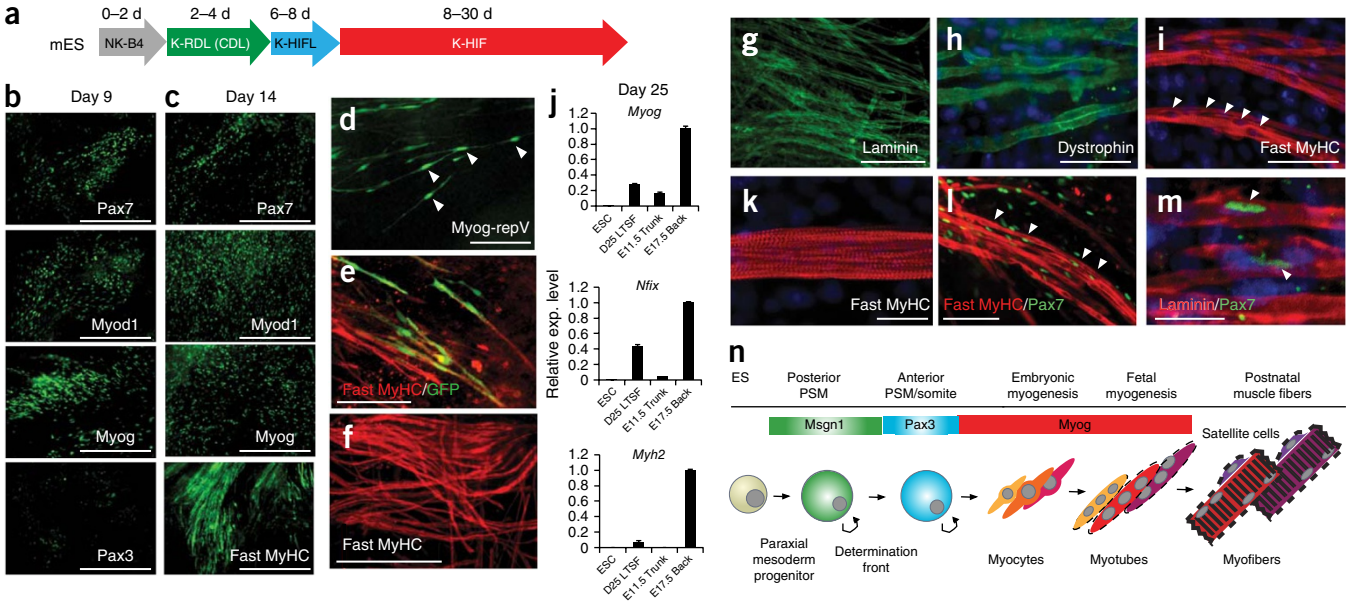

Figure 3 Differentiation of multinucleated striated muscle fibers and associated Pax7$^+$ cells from mouse ES cells *in vitro*. (**a**) The serum-free differentiation protocol of mES cells highlighting key factors applied during the differentiation and the time scale. N: N2 B27; B4: Bmp4; R: Rspo3; D: DMSO; C: Chir; L: LDN193189; H: HGF; I: IGF-1; F: FGF-2; K: KSR. (**b**,**c**) mES cells cultured for 9 d (**b**) and 14 d (**c**) in differentiation medium as shown in **a**. Immunohistochemistry with Pax7, Myod1, Myog, Pax3 and MyHC antibodies. Scale bars, 400 µm. (**d**) GFP live expression in Myog-repV culture differentiated for 9 d *in vitro*. Scale bar, 100 µm. Arrowheads, mononucleated Venus$^+$ myocytes. (**e**) Myog-repV cells differentiated for 9 d *in vitro* and stained for GFP (green) and fast MyHC (red). Note the transition stages between the GFP-only expressing myocytes to more mature MyHC expressing cells. Scale bar, 100 µm. (**f**) Mouse ES cells differentiated for 3 weeks *in vitro* and stained for fast MyHC. Scale bar, 400 µm. (**g**–**i**) Muscle fibers differentiated *in vitro* after 3 weeks of culture in serum-free differentiation medium stained for laminin (**g**), dystrophin (**h**) and fast MyHC (**i**). Note the continuous basal lamina deposit surrounding individual fibers (**g**), the subsarcolemmal accumulation of dystrophin (**h**) and the multinucleated fibers shown by DAPI counterstaining (**i**, arrowheads). Scale bars, 200 µm (**g**), 50 µm (**h**,**i**). (**j**) qRT-PCR analysis comparing expression levels of the myogenic markers *Myog*, *Nfix* and *Myh2* between ES cells, embryonic E11.5 trunk muscles, fetal E17.5 back muscles and ES cells differentiated for 25 d in serum-free myogenic conditions (D25 LTSF). E17.5 data are normalized to 1. Values are expressed as mean ± s.d. The ES-derived myogenic culture expresses *Myog*, *Nfix* and *Myh2* at significantly higher level when compared to E11.5 trunk muscles ($P < 0.005$). (**k**) Higher magnification of muscle fiber differentiated *in vitro* after 3 weeks of culture in serum-free differentiation medium, stained for fast MyHC and counterstained with DAPI showing the sarcomeric organization of the fibers. Scale bar, 25 µm. (**l**) Muscle fibers differentiated *in vitro* after 3 weeks of culture in differentiation medium, stained for fast MyHC (red) and Pax7 (green). Note Pax7$^+$ cells in close proximity to fibers (arrowheads). Scale bar, 100 µm. (**m**) Confocal section showing high magnification of a muscle fiber differentiated for 24 d *in vitro* labeled with an anti-laminin (red) and an anti-Pax7 antibody (green), showing a Pax7$^+$ nucleus inside the fiber basal lamina (arrowheads). Scale bar, 25 µm. (**n**) The major developmental stages of ES cell–derived paraxial mesoderm toward myogenic differentiation. Cellular phenotypes progression and the corresponding reporter genes phases used in this study to monitor the myogenic differentiation are also shown.

© 2015 Nature America, Inc. All rights reserved.

a posterior PSM-like fate. As Rspo3 is a Wnt activator, we replaced it with the GSK3β inhibitor CHIRON99021 (Chir), which also activates the Wnt pathway, in the differentiation medium (CDL). This led to similar induction of Msgn1$^+$ cells (**Fig. 2c**), which, when analyzed using quantitative real time PCR (qRT-PCR) and microarrays, showed a very similar profile to the cells differentiated in RDL medium (**Fig. 2d** and **Supplementary Fig. 2**).

In vivo, as paraxial mesoderm cells mature, they become located in the anterior PSM and downregulate expression of the posterior PSM markers *Msgn1* and *Tbx6* while activating expression of *Pax3*, an early and essential myogenic inducer expressed in the anterior PSM and in myogenic precursors[29] (**Figs. 1b** and **2a**). A similar dynamic was observed in culture in RDL or CDL medium as by day 5 of differentiation M$^+$ cells became Pax3$^+$ while downregulating Tbx6, suggesting acquisition of an anterior PSM fate (**Fig. 2g**). To monitor the differentiation of ES cells toward the anterior PSM fate, we generated a mouse ES reporter line (Pax3-GFP) in which GFP was placed under the control of *Pax3* regulatory sequences. When these reporter cells were cultured in RDL or CDL medium, ~30–50% of cells were GFP$^+$ after 6 d of differentiation (**Fig. 2c**). By qRT-PCR, the Pax3-GFP$^+$ (P$^+$) cells were essentially negative for the neural marker *Sox2* (**Fig. 2e**), but positive for the anterior PSM/somitic markers *Pax3*, *Tbx18*, *Meox2* and *Uncx* (**Fig. 2e**,**f**), thus excluding a neural origin for these cells. Expression levels of these genes were similar to endogenous expression levels in mouse embryonic tails (**Fig. 2f**). Furthermore, these cells expressed Pax3 (**Fig. 2h**) and had a typical mesenchymal morphology different from that of the epithelial rosette-forming neural precursors expressing *Pax3* observed in neural-inducing conditions (data not shown).

A comparison of global gene expression in P$^+$ cells differentiated in RDL medium and in the anterior PSM showed that during *in vitro* differentiation ES cells upregulated a large number of anterior PSM signature genes, including *Ripply2*, *Meox2*, *Pax3*, *Foxc2*, *Cer1* and *Dmrt2* (**Fig. 2j** and **Supplementary Table 3**). Very similar differentiation profiles were observed in P$^+$ cells differentiated in CDL medium (**Fig. 2f** and **Supplementary Fig. 2**). Thus, *in vitro* differentiation of the Msgn1-repV and the Pax3-GFP reporter ES cells in the presence of Wnt activators and BMP inhibitor efficiently recapitulates early differentiation stages of the paraxial mesoderm in the PSM, providing a scalable protocol for the generation of large numbers of cells that closely resemble the precursors of myogenic cells *in vivo*.

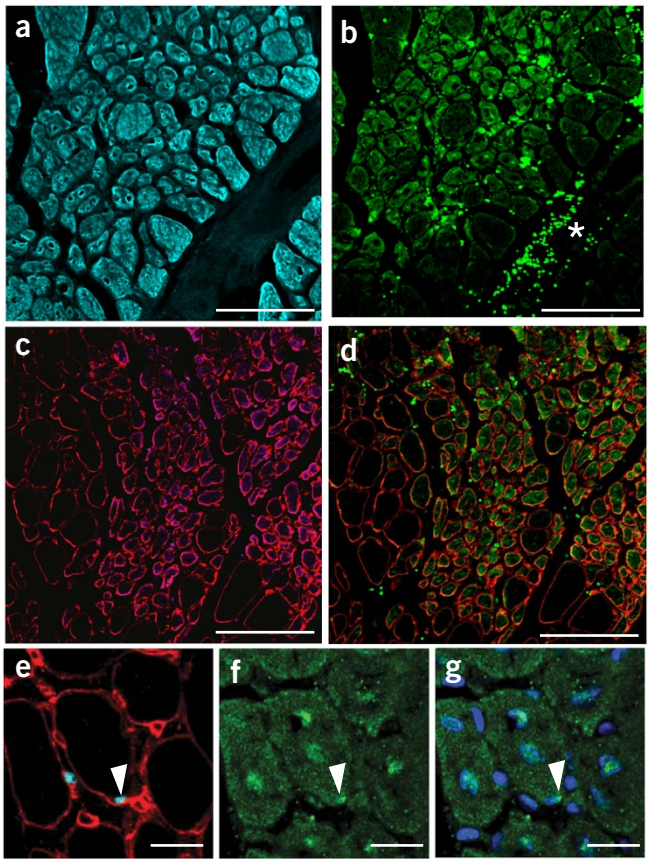

Figure 4 Graft of purified Pax7$^+$ cells differentiated *in vitro* into adult *mdx* muscles. (**a**–**g**) Confocal sections showing immunohistochemistry on transverse sections of transplanted tibialis anterior of 4-month-old Rag1$^{-/-}$ Dmd$^{mdx\text{-}5Cv}$ mice transplanted with FACS-sorted Pax7-GFP$^+$ cells from 3-week- (**a**–**d**) and 4-week- (**e**–**g**) old myogenic cultures. Grafted mice were analyzed after 1 month (**a**–**d**) or 2 months (**e**–**g**). Comparison of fast MyHC marking the muscle fibers (**a**) and of GFP expression labeling the engrafted fibers (**b**). The site of injection is assessed by the presence of the 2 µm tracking fluorescent beads (*). Comparison of dystrophin (purple) and laminin (red) (**c**) and GFP-labeled donor-derived fibers (**d**). All muscle fibers are surrounded by laminin but only GFP$^+$ fibers express dystrophin. (**e**) Pax7$^+$ nuclei (cyan, arrowhead) can be found under the basal lamina (red). (**f**) GFP labeling indicating donor origin of the fibers and Pax7$^+$ cell (green, arrowhead). (**g**) GFP and DAPI overlay showing the nuclear localization of GFP in fiber nuclei and in the Pax7$^+$ cell (arrowhead). Scale bars, 200 µm (**a**–**d**), 50 µm (**e**–**g**).

Recapitulation of primary fetal myogenesis *in vitro*

We next sought to define conditions to reproducibly differentiate the anterior PSM–like cells to skeletal muscle. During embryogenesis, the formation of muscle fibers starts with primary myogenesis, when muscle fibers expressing slow myosin heavy chain (MyHC) and harboring a small number of nuclei form from Pax3$^+$ precursors. This phase is then followed by fetal or secondary myogenesis, when Pax7$^+$ myogenic precursors derived from the Pax3$^+$ population fuse to form larger fibers harboring a large number of nuclei and expressing more mature MyHC isoforms, such as fast MyHC[29]. ES cells were differentiated in RDL or CDL medium for 6 d and then cultured in medium containing the myogenesis-promoting factors hepatocyte growth factor (HGF), insulin growth factor 1 (IGF-1) and fibroblast growth factor 2 (FGF-2)[30] for up to 2 months (**Fig. 3a**). At day 9, differentiating cells had downregulated Pax3 and begun to activate Pax7, as is observed for myogenic precursors *in vivo*[29]. At this stage, many cells had differentiated into proliferating myoblasts (Myod1$^+$, **Fig. 3b**) and myocytes (Myog$^+$, **Fig. 3b**). At day 10, the Myogenin$^+$ population accounted for 25–30% of the cells (**Fig. 2c**).

To monitor the appearance of committed skeletal muscle cells, we generated a reporter ES cell line, Myog-repV, harboring a 1.6-kb fragment of the *Myogenin1* promoter fused to Venus. Venus$^+$ myocytes with a single centrally located nucleus (**Fig. 3d**, arrowheads), strongly resembling early myotome cells produced during primary myogenesis, were detected after 1 week in culture. The number of cells expressing Pax7, Myod1, Myog and fast MyHC steadily increased during the second week of differentiation, covering large areas of the culture (**Fig. 3c**). The Myog-repV$^+$ primary myocytes progressively fused to produce fast MyHC$^+$ myotubes (**Fig. 3e**), extending up to several hundred micrometers by 10 d (data not shown). These results suggest that our protocol recapitulates essential steps of primary myogenesis.

After 2–3 weeks of culture, several thousand multinucleated laminin$^+$ and dystrophin$^+$ fibers expressing fast MyHC were observed per square centimeter in the cultures (**Fig. 3f**–**i** and **Supplementary Table 4**). After 3–4 weeks, the more mature (larger) fibers contained ~25–50 myonuclei, a number similar to that found in perinatal fibers[31] (**Supplementary Table 4**). We compared by qRT-PCR the expression of a set of myogenic markers in 3-week-old cultures differentiated in the conditions described above (**Fig. 3a**) with cultures of undifferentiated ES cells, and with mouse E11.5 trunk muscles (containing primary myofibers) and E17.5 back muscles (in which secondary, fetal myogenesis is ongoing) (**Fig. 3j**). Notably, the marker of fetal muscle fibers *Nfix*[32] and the *Fast2A* (*Myh2*) myosin heavy chain were not observed in E11.5 trunk muscles but were significantly enriched both in the E17.5 muscle sample and in the 25-day-old cultures (**Fig. 3j**; $P < 0.005$). The muscle fibers differentiated in culture for 3 to 4 weeks reached a density of ~40 fibers per square millimeter, with local fiber patches density reaching 300$^+$ fibers per square millimeter (**Supplementary Table 4**). Immuno-labeling with anti-fast MyHC antibody showed that these fibers exhibited highly organized striation as expected in mature muscle fibers (**Fig. 3k**). Differentiated fibers exhibited spontaneous *in vitro* contractions, indicating that the sarcomeric organization of the fibers was functional (data not shown). The fibers were >1 mm in length and ~11 µm in width, with a sarcomeric length of ~2.4 µm, similar to the dimensions of post-natal fibers *in vivo*[31] (**Supplementary Table 4**). Thus, our differentiation protocol recapitulates both primary and fetal (secondary) skeletal myogenesis, producing striated contractile muscle fibers exhibiting a phenotype similar to that of early post-natal fibers.

Satellite cell–like properties of Pax7$^+$ cells

In 3-week-old cultures, a population of small cells expressing Pax7 was found interspersed with the fast MyHC$^+$ fibers, as expected for myogenic precursors and satellite cells [33,34] (**Fig. 3l**). After 3–4 weeks in culture, the number of Pax7$^+$ cells decreased, and those that remained were tightly associated with the myofibers (**Fig. 3l**). Many of these cells were Ki67$^-$, suggesting that they had exited the cell cycle (data not shown), and they were sometimes found enclosed in the laminin$^+$ basal lamina surrounding the muscle fibers, as expected for satellite cells (**Fig. 3m**,**n**).

These data suggested that cells in the mature myogenic cultures spontaneously organized to recreate a niche for satellite cells. To test whether the Pax7$^+$ cells had properties of satellite cells, we generated a mouse Pax7-GFP transgenic ES cell reporter line in which GFP expression is driven by a Pax7 bacterial artificial chromosome transgene. We also introduced a ubiquitous reporter, CAGGS-CFP,

© 2015 Nature America, Inc. All rights reserved.

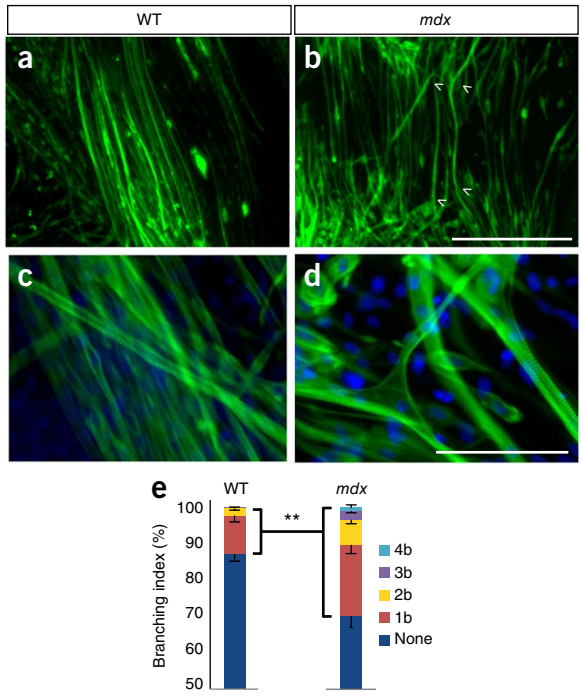

Figure 5 Muscle fibers differentiated *in vitro* from dystrophin-deficient *mdx* ES cells show an abnormal branching phenotype. (**a**–**d**) Comparison between control (**a**,**c**) and *mdx* (**b**,**d**) muscle fibers differentiated *in vitro* and labeled with an antibody against fast MyHC showing the branched phenotype (arrowheads) of *mdx* fibers. Scale bars, 500 µm (**a**,**b**), 100 µm (**c**,**d**). (**e**) Comparison of the branching index (in %) of control and *mdx* fibers *in vitro*. Fibers are categorized by number of branches. Error bars, mean ± s.d. Fisher's exact test, $^{**}P \leq 0.005$.

in these cells to permanently track their progeny in grafting experiments. We differentiated these cells for 3–4 weeks according to the protocol described above and sorted the Pax7-GFP$^+$ cells by flow cytometry, which represented about 0.5% of the total single-cell population. Next we grafted ~1 × 10^5 cells into the tibialis anterior muscle of adult Rag1$^{-/-}$ Dmd$^{mdx\text{-}5Cv}$ (*mdx*) mice, which are immunodeficient mice lacking dystrophin. One month after injection, the GFP-expressing donor cells had generated foci of fibers that were fast MyHC$^+$ (**Fig. 4a**,**b**) and dystrophin$^+$ (**Fig. 4c**,**d**). The grafted cells also gave rise to Pax7$^+$ satellite cell–like cells located under the basal lamina of GFP$^+$ fibers (**Fig. 4e**–**g**). The donor-derived fibers were well aligned with host fibers and had a smaller cross-sectional area compared with host GFP$^-$ fibers (**Fig. 4a**–**d**). These experiments demonstrate that the Pax7$^+$ cells generated *in vitro* can behave as satellite cells when grafted in a dystrophin-deficient environment.

Branching of differentiated dystrophin-deficient fibers

We next derived ES cell lines from blastocysts of *mdx* mice. After 3–5 weeks of myogenic differentiation *in vitro* in the serum-free conditions described above (**Fig. 3a**), *mdx* ES cells differentiated to mature muscle fibers. Multinucleated *mdx* fibers reached up to 1.2 mm in length, with an average diameter of 10.5 µm, values similar to those of the control fibers. Spontaneously contracting fibers were also observed in differentiated *mdx* ES cell cultures (data not shown).

It has been suggested that lack of dystrophin weakens the fiber membrane, causing it to tear upon contraction and leading ultimately to fiber necrosis[35,36]. To test whether *in vitro*–generated *mdx* fibers exhibit defects in membrane integrity, we stained 3- to 4-week-old fibers with Evans blue[37]. Dye uptake was not detected in *mdx* or in control fibers, whereas it was observed following membrane permeabilization with saponin, suggesting that membrane integrity was not impaired (**Supplementary Fig. 3**). However, ~30% of the *mdx* muscle fibers had one or more lateral branches (**Fig. 5b**,**d**,**e**) compared to only ~10% of control fibers (**Fig. 5a**,**c**). Fibers with multiple branches, which created a star-like aspect, were essentially restricted to *mdx* cultures (**Fig. 5d**,**e**; $P < 0.005$). Although sarcomeres appeared grossly normal, with an average length of 2.4 µm, bundling of the myofibrils along the *mdx* fibers was often disrupted, presenting tilts or twists (**Fig. 5d**) resembling those reported for *mdx* fibers *in vivo*[38].

Myogenic differentiation of human iPS cells

Finally, we adapted our myogenic differentiation conditions to human induced pluripotent stem (hiPS) cells. We first cultured hiPS cells as single cells for 6 d in serum-free medium containing Chir and LDN193189, followed by culture in serum-free medium containing IGF-1, HGF and FGF-2 growth factors (**Fig. 6a**). After 20 d, the cultures contained large fields comprising fast MyHC$^+$ (**Fig. 6b**,**e**) and Myogenin$^+$ (**Fig. 6c**) fibers and PAX7$^+$ cells (**Fig. 6d**). Between 20 and 30 d of culture, large numbers of MyHC$^+$ fibers more than one mm long intermingled with PAX7$^+$ cells appeared (**Fig. 6d**–**f**, data not shown). By 4 weeks, ~22% of nuclei were MYOG$^+$ and 23% of nuclei were PAX7$^+$. The muscle fibers showed organized sarcomeres, as demonstrated by the periodic distribution of the sarcomeric proteins Titin and fast MyHC (**Fig. 6h**–**j**). Furthermore,

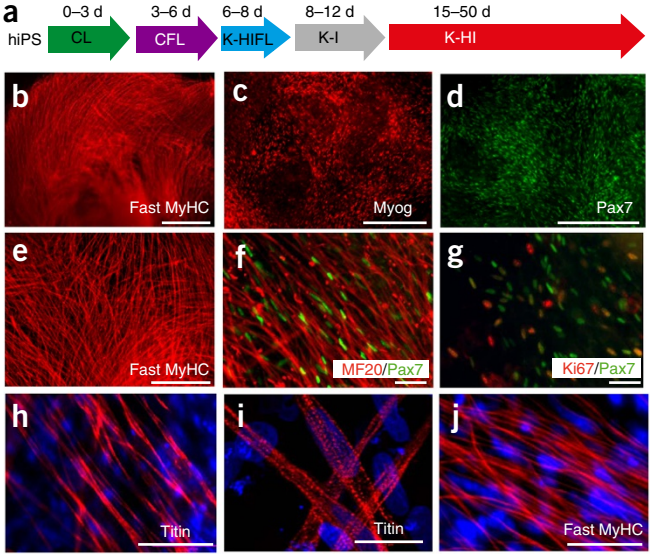

Figure 6 Myogenic differentiation of human iPS cells. (**a**) Schematic representation of the serum-free differentiation protocol highlighting key factors applied during the differentiation and the time scale. C: Chir; L: LDN193189; F: FGF-2; K: KSR; H: HGF; I: IGF-1. (**b**–**d**) hiPS cells were differentiated as indicated. Cells were fixed after 3 weeks of differentiation and stained for fast MyHC (**b**), Myogenin (**c**) and Pax7 (**d**). Scale bars, 1,000 µm. (**e**–**g**) hiPS cell culture after 40 d of myogenic differentiation, stained for fast MyHC (**e**; scale bar, 500 µm), or double-stained for MF20/Pax7 (**f**) and Ki67/Pax7 (**g**) (scale bars, 100 µm). (**h**–**j**) Muscle fibers differentiated *in vitro* in long-term serum-free cultures and stained for Titin (**h**) and the fast MyHC (**j**) (scale bars, 200 µm), with a high-magnification confocal image (**i**) showing the periodic organization of sarcomeres (scale bar, 20 µm).

© 2015 Nature America, Inc. All rights reserved.

these striated fibers exhibited spontaneous twitching, indicating that their sarcomeric organization was functional (**Supplementary Movie 1**). The diameter of the human muscle fibers generated *in vitro* was ~3.5 µm, that is, smaller than that of mouse fibers despite a similar length (**Supplementary Table 4**). Many of the PAX7$^+$ cells were also Ki67$^-$ and were often found lining the MyHC$^+$ fibers (**Fig. 6f**). The total number of PAX7$^+$ cells strongly decreased after 40 d down to ~1% at day 50.

With mouse cells, 7,000–10,000 multinucleated muscle fibers could be obtained in wells initially seeded with 20,000 ES cells, whereas with human cells we obtained around 50,000–70,000 fibers starting from 75,000 hiPS cells. These yields compare well with current cardiomyocyte differentiation protocols (**Supplementary Table 4**)[39]. Similar differentiation efficiencies were also observed with the human ES cell line H9 (data not shown). We directly compared our protocol with that of reference 24, in which no BMP inhibitor was added in the first phase of the culture. After 30 d we were unable to detect significant amounts of MyHC$^+$ fibers or PAX7$^+$ cells in hiPS cells cultured with these conditions. Small fast MyHC$^+$ myotubes were detected only after 50 d in culture, but they did not show any striation (**Supplementary Fig. 4**).

DISCUSSION

Difficulties in differentiating human pluripotent cells toward a myogenic fate have hampered the development of *in vitro* models of muscle diseases such as sarcopenia, cachexia and muscular dystrophies. Here we report the *in vitro* differentiation of mouse and human pluripotent cells into striated, linear, millimeter-long muscle fibers. The fibers can contract, and they provide a niche that supports the emergence of Pax7$^+$ cells that resemble satellite cells. The Pax7$^+$ cells are mostly found along the membrane of differentiated muscle fibers, often under the laminin$^+$ basal lamina, and a majority of them are quiescent, as expected for satellite cells. Such fibers do not form in standard myoblast monolayer cultures, in which much shorter, irregularly shaped myotubes lacking striation are usually observed. One reason for the difference between these two types of culture might be that our protocol recapitulates the entire myogenic developmental sequence. *In vivo*, primary fibers serve as a scaffold for secondary fibers, which organize the linear fusion of myoblastic cells to form adult muscle fibers[40]. In our cultures, we observe formation of primary and secondary muscle fibers, suggesting that such a morphogenetic sequence takes place. These events might also be critical to the emergence of Pax7$^+$ cells with satellite cell properties. Similar self-organizing processes in differentiated ES cell cultures are now widely recognized for a number of structures, such as the retina[41] and the gut[42], and thus likely occur for muscle tissue as well.

We used four fluorescent reporter ES cell lines to systematically optimize the differentiation of mouse ES cells toward a paraxial mesoderm fate on the basis of developmental cues. Transposition of the protocol to human pluripotent cells required several modifications but retained the key elements of the mouse method. In particular, human ES cells being equivalent to mouse epiblast cells[43], the first step of the mouse protocol aimed at inducing epiblast from 'naive' mouse ES cells was unnecessary. Thus, hiPS cells were directly exposed to Wnt activation and to inhibition of the BMP pathway. We found that strong BMP inhibition at this stage is critical, as otherwise cells begin to express BMP4 and drift to a lateral plate fate (data not shown). This step represents a major difference from protocols for paraxial mesoderm induction in which only Wnt signaling is activated[14,20,22–24]. We also found that early addition of FGF-2 is beneficial to the survival and proliferation of the human pluripotent cells. After mouse and human pluripotent cells were induced to a mature PSM fate, exposure to the three myogenic growth factors HGF, IGF-1 and FGF-2 (ref. 30) resulted in myogenesis. Mouse myotubes were detected after 1 –2 weeks of differentiation, whereas human cell cultures required ~3 weeks, consistent with the generally slower differentiation of human pluripotent cells compared with mouse ES cells. Although virtually nothing is known about the early stages of paraxial mesoderm development and myogenesis in humans, our data suggest that signaling cues similar to those described for mouse are deployed during development of the human muscle lineage.

Our work on *mdx* ES cells suggests that dystrophin is required for normal morphogenesis of muscle fibers, at least in culture[44], and provides a tractable *in vitro* model to study the cell biology of DMD. Increased branching of myofibers has been reported in DMD patients, in embryonic and adult *mdx* mice and in mice lacking the olfactory receptor MOR23 or the intermediate filament desmin[44–47]. In adult *mdx* mice, increased branching has been proposed to result from abnormal fiber morphogenesis caused by defective myoblast fusion arising during the regeneration process stimulated by fiber degeneration[36,45,47]. However, the increased branching of *mdx* fibers differentiated from ES cells *in vitro* was unexpected as such a phenotype has not been reported in primary *mdx* myoblast cultures or in human DMD myoblast cultures. Our observation of a branching defect may be explained by the capacity of cells generated by the present protocol to self-organize into long fibers. Our model will allow analysis of whether this defect originates in fusion of myogenic precursors.

Healthy muscle precursors grafted into *mdx* mice give rise to considerable numbers of dystrophin-expressing fibers[48]. However, clinical trials using human myoblasts amplified *in vitro* have failed owing to poor engraftment of the cells[49]. Mouse studies to date have established that the cell type with the best regenerative properties is the Pax7$^+$ satellite cell[48,50]. Our protocol for differentiating mouse ES cells to a muscle fate produces Pax7$^+$ satellite cell–like cells capable of generating dystrophin$^+$ muscle fibers and their associated satellite cells when grafted in *mdx* mice muscle. Further optimization of the protocol for human pluripotent cells may facilitate the development of cell therapies for DMD and other degenerative diseases of the muscle.

METHODS

Methods and any associated references are available in the online version of the paper.

Accession codes. GEO: GSE39615.

Note: Any Supplementary Information and Source Data files are available in the online version of the paper.

ACKNOWLEDGMENTS

We thank C. Henderson, K. Hnia, M. Knockaert and members of the Pourquié laboratory for comments. We are grateful to J. Pace, T. Knauer-Meyer, G. Vilhais-Neto, and M. McLaird for help. We thank C. Ebel, C. Thibault-Carpentier, A. Magloth-Roth and the Imaging Facility. We thank the microinjection and phenotyping teams of the Mouse Clinical Institute. We thank M. Durnin from the Stowers Institute Cell Culture and Animal Facilities. This work was supported by an advanced grant from the European Research Council to O.P., by the Stowers Institute for Medical Research, by the Howard Hughes Medical Institute, by the FP7 EU grant Plurimes (agreement no. 602423) and by a strategic grant from the French Muscular Dystrophy Association (AFM) to O.P. The Venus Plasmid was a kind gift of A. Miyawaki. The anti-Tbx6 antibody was a kind gift of Y. Saga[51].

AUTHOR CONTRIBUTIONS

J.C. designed and performed experiments, analyzed data and coordinated the project. M.O. performed the PSM microdissection series. Z.A.T. transposed

© 2015 Nature America, Inc. All rights reserved.

the differentiation protocol to hiPS cells and characterized the human cultures with help from C.M. and B.G. B.G., A.M. and G.G. carried out most of the mouse ES cell differentiation experiments, and M.H. carried out hiPS cell and hES cell experiments, under J.C.'s supervision. O.S. validated the Myog-repV line. A.H. helped coordinate experiments. F.B. contributed to hiPS cell culture and differentiation. Y.Z. helped develop the serum-free protocol. P.M. and O.T. helped with microarray data analysis. T.C. helped analyze *mdx* cultures. A.B. contributed experimentally to the early project. L.K. provided technical support. J.-M.G. generated reporter constructs. S.H., B.D. and F.R. provided the Pax3-GFP ES cells. B.G.-M. and S.T. provided expertise and the Pax7-GFP ES cells. S.V. helped establish *mdx* ES cells. E.G. provided Rag1-*mdx* mice and performed transplantation. O.P. conceived and supervised the overall project. O.P. and J.C. performed the final data analysis and wrote the manuscript.

COMPETING FINANCIAL INTERESTS

The authors declare competing financial interests: details are available in the online version of the paper.

Reprints and permissions information is available online at http://www.nature.com/reprints/index.html.

1. Rinaldi, F. & Perlingeiro, R.C. Stem cells for skeletal muscle regeneration: therapeutic potential and roadblocks. *Transl. Res.* **163**, 409–417 (2013).
2. Darabi, R. *et al.* Human ES- and iPS-derived myogenic progenitors restore DYSTROPHIN and improve contractility upon transplantation in dystrophic mice. *Cell Stem Cell* **10**, 610–619 (2012).
3. Darabi, R. *et al.* Functional skeletal muscle regeneration from differentiating embryonic stem cells. *Nat. Med.* **14**, 134–143 (2008).
4. Albini, S. *et al.* Epigenetic reprogramming of human embryonic stem cells into skeletal muscle cells and generation of contractile myospheres. *Cell Reports* **3**, 661–670 (2013).
5. Salani, S. *et al.* Generation of skeletal muscle cells from embryonic and induced pluripotent stem cells as an *in vitro* model and for therapy of muscular dystrophies. *J. Cell. Mol. Med.* **16**, 1353–1364 (2012).
6. Tanaka, A. *et al.* Efficient and reproducible myogenic differentiation from human iPS cells: prospects for modeling Miyoshi Myopathy *in vitro*. *PLoS ONE* **8**, e61540 (2013).
7. Abujarour, R. *et al.* Myogenic differentiation of muscular dystrophy-specific induced pluripotent stem cells for use in drug discovery. *Stem Cells Transl. Med.* **3**, 149–160 (2014).
8. Braun, T. & Arnold, H.H. ES-cells carrying two inactivated myf-5 alleles form skeletal muscle cells: activation of an alternative myf-5-independent differentiation pathway. *Dev. Biol.* **164**, 24–36 (1994).
9. Rohwedel, J. *et al.* Muscle cell differentiation of embryonic stem cells reflects myogenesis *in vivo*: developmentally regulated expression of myogenic determination genes and functional expression of ionic currents. *Dev. Biol.* **164**, 87–101 (1994).
10. Braun, T. & Arnold, H.H. Myf-5 and myoD genes are activated in distinct mesenchymal stem cells and determine different skeletal muscle cell lineages. *EMBO J.* **15**, 310–318 (1996).
11. Zheng, J.K. *et al.* Skeletal myogenesis by human embryonic stem cells. *Cell Res.* **16**, 713–722 (2006).
12. Mizuno, Y. *et al.* Generation of skeletal muscle stem/progenitor cells from murine induced pluripotent stem cells. *FASEB J.* **24**, 2245–2253 (2010).
13. Tanaka, M. *et al.* BMP inhibition stimulates WNT-dependent generation of chondrogenic mesoderm from embryonic stem cells. *Stem Cell Res. (Amst.)* **3**, 126–141 (2009).
14. Hwang, Y. *et al.* Directed *in vitro* myogenesis of human embryonic stem cells and their *in vivo* engraftment. *PLoS ONE* **8**, e72023 (2013).
15. Chang, H. *et al.* Generation of transplantable, functional satellite-like cells from mouse embryonic stem cells. *FASEB J.* **23**, 1907–1919 (2009).
16. Xu, C. *et al.* A zebrafish embryo culture system defines factors that promote vertebrate myogenesis across species. *Cell* **155**, 909–921 (2013).
17. Sakurai, H. *et al. In vitro* modeling of paraxial mesodermal progenitors derived from induced pluripotent stem cells. *PLoS ONE* **7**, e47078 (2012).
18. Sakurai, H. *et al.* Bidirectional induction toward paraxial mesodermal derivatives from mouse ES cells in chemically defined medium. *Stem Cell Res. (Amst.)* **3**, 157–169 (2009).
19. Sakurai, H., Okawa, Y., Inami, Y., Nishio, N. & Isobe, K. Paraxial mesodermal progenitors derived from mouse embryonic stem cells contribute to muscle regeneration via differentiation into muscle satellite cells. *Stem Cells* **26**, 1865–1873 (2008).
20. Borchin, B., Chen, J. & Barberi, T. Derivation and FACS-mediated purification of PAX3+/PAX7+ skeletal muscle precursors from human pluripotent stem cells. *Stem Cell Reports* **1**, 620–631 (2013).
21. Hosoyama, T., McGivern, J.V., Van Dyke, J.M., Ebert, A.D. & Suzuki, M. Derivation of myogenic progenitors directly from human pluripotent stem cells using a sphere-based culture. *Stem Cells Transl. Med.* **3**, 564–574 (2014).
22. Gouti, M. *et al. In vitro* generation of neuromesodermal progenitors reveals distinct roles for wnt signalling in the specification of spinal cord and paraxial mesoderm identity. *PLoS Biol.* **12**, e1001937 (2014).
23. Tan, J.Y., Sriram, G., Rufaihah, A.J., Neoh, K.G. & Cao, T. Efficient derivation of lateral plate and paraxial mesoderm subtypes from human embryonic stem cells through GSKi-mediated differentiation. *Stem Cells Dev.* **22**, 1893–1906 (2013).
24. Shelton, M. *et al.* Derivation and expansion of PAX7-positive muscle progenitors from human and mouse embryonic stem cells. *Stem Cell Rev.* **3**, 516–529 (2013).
25. Ozbudak, E.M., Tassy, O. & Pourquie, O. Spatiotemporal compartmentalization of key physiological processes during muscle precursor differentiation. *Proc. Natl. Acad. Sci. USA* **107**, 4224–4229 (2010).
26. Wittler, L. *et al.* Expression of Msgn1 in the presomitic mesoderm is controlled by synergism of WNT signalling and Tbx6. *EMBO Rep.* **8**, 784–789 (2007).
27. Kazanskaya, O. *et al.* R-Spondin2 is a secreted activator of Wnt/beta-catenin signaling and is required for Xenopus myogenesis. *Dev. Cell* **7**, 525–534 (2004).
28. Tonegawa, A., Funayama, N., Ueno, N. & Takahashi, Y. Mesodermal subdivision along the mediolateral axis in chicken controlled by different concentrations of BMP-4. *Development* **124**, 1975–1984 (1997).
29. Hutcheson, D.A., Zhao, J., Merrell, A., Haldar, M. & Kardon, G. Embryonic and fetal limb myogenic cells are derived from developmentally distinct progenitors and have different requirements for beta-catenin. *Genes Dev.* **23**, 997–1013 (2009).
30. Chargé, S.B. & Rudnicki, M.A. Cellular and molecular regulation of muscle regeneration. *Physiol. Rev.* **84**, 209–238 (2004).
31. White, R.B., Bierinx, A.S., Gnocchi, V.F. & Zammit, P.S. Dynamics of muscle fibre growth during postnatal mouse development. *BMC Dev. Biol.* **10**, 21 (2010).
32. Messina, G. *et al.* Nfix regulates fetal-specific transcription in developing skeletal muscle. *Cell* **140**, 554–566 (2010).
33. Relaix, F., Rocancourt, D., Mansouri, A. & Buckingham, M.A. Pax3/Pax7-dependent population of skeletal muscle progenitor cells. *Nature* **435**, 948–953 (2005).
34. Sambasivan, R. & Tajbakhsh, S. Skeletal muscle stem cell birth and properties. *Semin. Cell Dev. Biol.* **18**, 870–882 (2007).
35. Rahimov, F. & Kunkel, L.M. The cell biology of disease: cellular and molecular mechanisms underlying muscular dystrophy. *J. Cell Biol.* **201**, 499–510 (2013).
36. Allen, D.G. & Whitehead, N.P. Duchenne muscular dystrophy--what causes the increased membrane permeability in skeletal muscle? *Int. J. Biochem. Cell Biol.* **43**, 290–294 (2011).
37. Matsuda, R., Nishikawa, A. & Tanaka, H. Visualization of dystrophic muscle fibers in mdx mouse by vital staining with Evans blue: evidence of apoptosis in dystrophin-deficient muscle. *J. Biochem.* **118**, 959–964 (1995).
38. Friedrich, O. *et al.* Microarchitecture is severely compromised but motor protein function is preserved in dystrophic mdx skeletal muscle. *Biophys. J.* **98**, 606–616 (2010).
39. Minami, I. *et al.* A small molecule that promotes cardiac differentiation of human pluripotent stem cells under defined, cytokine- and xeno-free conditions. *Cell Rep.* **2**, 1448–1460 (2012).
40. Biressi, S., Molinaro, M. & Cossu, G. Cellular heterogeneity during vertebrate skeletal muscle development. *Dev. Biol.* **308**, 281–293 (2007).
41. Eiraku, M. *et al.* Self-organizing optic-cup morphogenesis in three-dimensional culture. *Nature* **472**, 51–56 (2011).
42. McCracken, K.W. *et al.* Modelling human development and disease in pluripotent stem-cell-derived gastric organoids. *Nature* **516**, 400–404 (2014).
43. Li, W. & Ding, S. Human pluripotent stem cells: decoding the naive state. *Sci. Transl. Med.* **3**, 76ps10 (2011).
44. Merrick, D., Stadler, L.K., Larner, D. & Smith, J. Muscular dystrophy begins early in embryonic development deriving from stem cell loss and disrupted skeletal muscle formation. *Dis. Model. Mech.* **2**, 374–388 (2009).
45. Chan, S. & Head, S.I. The role of branched fibres in the pathogenesis of Duchenne muscular dystrophy. *Exp. Physiol.* **96**, 564–571 (2011).
46. Goodall, M.H., Ward, C.W., Pratt, S.J., Bloch, R.J. & Lovering, R.M. Structural and functional evaluation of branched myofibers lacking intermediate filaments. *Am. J. Physiol. Cell Physiol.* **303**, C224–C232 (2012).
47. Pavlath, G.K. A new function for odorant receptors: MOR23 is necessary for normal tissue repair in skeletal muscle. *Cell Adh. Migr.* **4**, 502–506 (2010).
48. Montarras, D. *et al.* Direct isolation of satellite cells for skeletal muscle regeneration. *Science* **309**, 2064–2067 (2005).
49. Mouly, V. *et al.* Myoblast transfer therapy: is there any light at the end of the tunnel? *Acta Myol.* **24**, 128–133 (2005).
50. Collins, C.A. *et al.* Stem cell function, self-renewal, and behavioral heterogeneity of cells from the adult muscle satellite cell niche. *Cell* **122**, 289–301 (2005).
51. Yasuhiko, Y. *et al.* Tbx6-mediated Notch signaling controls somite-specific Mesp2 expression. *Proc. Natl. Acad. Sci. USA* **103**, 3651–3656 (2006).

© 2015 Nature America, Inc. All rights reserved.

ONLINE METHODS

Generation of mouse reporter and *mdx* ES cell line. *Msgn1-repV line.* The Msgn1-repV transgene consists of a 6.5-kb fragment of the mouse *Mesogenin1* promoter[26] inserted upstream of the Venus (YFP) coding sequence[52] followed by the SV40 poly-adenylation sequence and a neomycin resistance cassette flanked by FRT sites. Mouse ES cells (E14, 129P2 genetic background, BayGenomics) were transfected with the linearized construct using Lipofectamin (Invitrogen). Clones were selected for Neomycin resistance and validated by the tetraploid aggregation technique as described[53]. One clone, called Msgn1-repV, showing the appropriate expression pattern was selected for further studies.

Pax3-GFP line. Pax3-GFP ES cells were generated by homologous recombination using a targeting construct derived from that described in[54]. Briefly, the Pax3-GFP *(Gene X-IRESnLacZ)* allele contains 2.4 kb of the 5′ genomic region of *Pax3*, but lacks the coding sequence of exon 1, and 4 kb of the 3′ sequence which contains exons 2–4. The insert construct is composed of the coding sequence for GFP, followed by a Puromycin selection cassette flanked by FRT sites. The targeting vector was electroporated into CK 35 ES cells (129Sv genetic background)[55]. ES cells were selected and screened for recombination events by Southern blot analysis using EcoRV digestion and a 5′-flanking probe. The positive clones were further verified by using 3′ external and internal probes. Targeted ES cells were recovered with a 0.5% frequency, and efficient germline transmission was used to assay cells' pluripotency. In order to generate Pax3-GFP ES cells, targeted ES cells were electroporated with a construct containing the FLP recombinase.

Myog-repV line. The same strategy as for Msgn1-repV was used with the Myog-repV transgene using a 1.6-kb fragment of the mouse *Myogenin* promoter[56]. One clone, called Myog-repV, showed colocalization of the fluorescent reporter with the endogenous Myogenin protein in myocytes differentiated from embryoid bodies as described[9] and was selected for further studies.

Pax7-GFP blue line. Pax7-GFP mES clones were derived from the transgenic mice Tg: Pax7-nGFP described in[57]. Cells were cultured in medium containing 1 μM PD0325901 (Tocris, Stemgent) and 3 μM CHIRON99021 (Chir, Tocris, Stemgent) (2i medium) as described[58]. Cells were transfected with an ubiquitous reporter construct composed of CAGG-nlsCFP followed by the SV40 poly-adenylation sequence and a puromycin resistance cassette flanked by FRT sites. Picked clones were isolated and further amplified by passages in 2i medium. Two clones were further selected for myogenic differentiation and grafting experiments. The Pax7-GFP label is necessary to sort the cells to be grafted and the CFP label is required to track the descendants of these cells in the host. Thus muscle fibers deriving from the grafted Pax7$^+$ cells are expected to express only CFP whereas satellite cells derived from the grafted cells are expected to express both GFP and CFP. While GFP and CFP expression is expected to be nuclear we have observed leakage of the fluorescent proteins to the sarcoplasm of muscle fibers in which both cytoplasmic and nuclear staining was observed.

Mdx ES cells. mdx mES clones were derived from the dystrophin mutant *mdx* homozygous/hemizygous blastocysts of the C57BL/10 genetic background (Jackson laboratory) cultured in 2i medium as described[58]. Ten clones were isolated by picking and further amplified by passages in 2i medium. Two clones (male, hemizygous) were further selected for the myogenic differentiation study. Labeling of the muscle fibers derived from the *mdx* ES cells with an anti-dystrophin antibody confirmed the absence of the protein (data not shown).

Mouse ES Cell culture and differentiation. *Maintenance.* Undifferentiated mouse ES cells were cultured on feeders of mitomycin-C inactivated mouse embryonic fibroblasts at 37 °C in 5% CO_2, in a maintenance medium composed of DMEM supplemented with 15% fetal bovine serum (Millipore), penicillin, streptomycin, 2 mM L-glutamine, 0.1 mM nonessential amino acids, 0.1% β-mercaptoethanol, 1,500 U/ml LIF and 2i inhibitors[58]. Cells were passaged by trypsinization (Invitrogen). Prior to differentiation, cells were passaged once onto gelatin-coated, feeder-free culture plates.

Serum-free differentiation of mouse ES cells toward a PSM-like fate. ES cells were trypsinized and plated at various densities in gelatin-coated, feeder-free, 96, 24 and 6-well plates directly in serum-free N2B27 medium supplemented with 1% Knock-out Serum Replacement (KSR, Gibco), 0.1% bovine serum albumin (Gibco) and BMP4 at 10 ng/ml (Peprotech) for 2 d. Cells were then changed to a DMEM-based medium, with 15% KSR, supplemented with recombinant 10 ng/ml Rspo3 (Peprotech, R&D Biosystems), 0.5% DMSO (Sigma), and 0.1 μM LDN193189 (Tocris, Miltenyi Biotec/Stemgent) (RDL medium) for 4 d. Alternatively, Rspo3 was replaced with CHIRON99021 (Chir; Tocris, Stemgent) at 1 μM. Differentiation experiments were performed at least 20 times independently.

Serum-free Myogenic differentiation of the mouse PSM-like cells. After the 4 d of culture in RDL or CDL medium, cells were changed to a DMEM-based medium with 15% KSR, 0.1% BSA supplemented with 10 ng/ml HGF, 2 ng/ml IGF-1, 20 ng/ml FGF-2 (Peprotech, R&D Biosystems) and 0.1 μM LDN193189 (HIFL medium) for 2 d. After day 8 of differentiation, only HGF, IGF-1, FGF-2 were supplemented (HIF medium). Media was changed every other day. Long–term differentiation experiments were performed at least 15 times independently, on more than five different mouse ES cell lines.

Human PS cell culture and differentiation. *Maintenance.* Undifferentiated human hiPS 11a[59] and H9 (ref. 60) hES cells were cultured on Matrigel (BD Biosciences)-coated dishes in mTeSR1 media (Stem Cell Technologies). Cells were passaged as aggregates.

Serum-free myogenic differentiation of the human iPS cells. Human iPS cell colonies were dissociated with Accutase (Stemcell Technologies) and plated as single cells per well on Matrigel -coated 24 and 12-well plates (approximately 15,000–18,000 cells/cm^2) in mTeSR1 supplemented with ROCK inhibitor (Y-27632, Sigma) for one day. The medium was changed to a DMEM-based medium supplemented with Insulin-Transferrin-Selenium (ITS, Gibco), 3 μM CHIRON99021 (Axon MedChem, Tocris) and 0.5 μM LDN193189 (Miltenyi Biotec/Stemgent) (CL medium). At day 3, 20 ng/ml FGF-2 (R&D Systems) was added for additional 3 d. After 6 d of differentiation, cells were changed to a DMEM-based medium supplemented with 10 ng/ml HGF, 2 ng/ml IGF-1, 20 ng/ml FGF-2 (R&D Systems) and 0.5 μM LDN193189 (HIFL medium) for 2 d. After day 8 of differentiation, cells were cultured in DMEM, 15% KSR, supplemented with 2 ng/ml IGF1 for 4 d, and then supplemented with both 10 ng/ml HGF and 2 ng/ml IGF-1 after day 12. Media was changed every day until day 12, and every second day thereafter. Long–term differentiation experiments were performed at least 15 times independently, on 2 unrelated hiPS and one hES lines. All human iPS and ES cell experiments were done according to local regulations (IGBMC and Brigham and Women's Hospital) and in agreement with national and international guidelines.

Flow cytometry analysis and FACS. *Analysis.* Cells were dissociated by trypsinization and analyzed by flow cytometry on a FACS calibur (BD Biosciences) according to GFP expression. Gating was determined for each reporter line using corresponding undifferentiated culture as a baseline control. Data are represented as % of GFP$^+$ cells in the culture.

Sorting. Msgn1-repV$^+$ (M$^+$) and Pax3-GFP$^+$ (P$^+$) cells were isolated by FACS from Msgn1-repV and Pax3-GFP cells respectively differentiated for 4 d and 6 d in RDL (or CDL) medium. Biological triplicates were generated. Gated fractions were sorted either on FACS Aria (BD Biosciences) or S3 cell sorter (Bio-Rad). Pax7-GFP$^+$ cells were isolated from the Pax7-GFP blue ES line differentiated for 3-4 weeks in serum-free medium. Data were further analyzed with the FlowJo software. Sorted populations were either processed for microarray analysis, qRT-PCR or for transplantation experiments.

Quantitative RT-PCR. Total RNA was extracted from ES cell cultures using Trizol (Invitrogen) or with the RNeasy micro-kit (Qiagen). RT-PCR was performed on 5 ng total RNA using QuantiFast SYBR Green RT-PCR Kit (Qiagen) and gene-specific primers (Primerbank) and run on a LightCycler 480II (Roche). Beta-actin was used as an internal control. For mouse tail/PSM reference, mouse E9.5 tails were microdissected posterior to the level of the forming somite (S0) and pooled for total RNA extraction. For embryonic and fetal muscle references, mouse E11.5 trunk muscles and mouse E17.5 back muscles were microdissected for total RNA extraction.

Microarrays generation and analysis. *Generation of the PSM microarray series.* Microdissections of CD1 mouse E9.5 embryos were done essentially

© 2015 Nature America, Inc. All rights reserved.
npg

doi:10.1038/nbt.3297

as described[61]. Caudo-rostral series of consecutive ~100 µm fragments were collected. 3 series of 7 fragments were generated, from the tail bud to the newly formed somite (S0) level (**Fig. 1a**,**b**). RNA from each fragment was extracted with Trizol (Invitrogen) and used to generate probes hybridized on GeneChip Mouse Genome 430 2.0 arrays.

Microarrays. Biotinylated cRNA targets were prepared from total RNA using a double amplification protocol according to the GeneChip Expression Analysis Technical Manual: Two-Cycle Target Labeling Assay (P/N 701021 Rev.5, Affymetrix, Santa Clara, USA). Following fragmentation, cRNAs were hybridized for 16 h at 45 °C on GeneChip Mouse Genome 430 2.0 arrays. Each microarray was then washed and stained on a GeneChip fluidics station 450 and further scanned with a GeneChip Scanner 3000 7G. Finally, raw data (.CEL Intensity files) were extracted from the scanned images using the Affymetrix GeneChip Command Console (AGCC) version 3.1.

Microarray data analysis. Initial filtering and preprocessing, including background correction, quantile normalization and summarization, was performed using both RMA and MAS with the R Bioconductor package (R version 2.12.1, Bioconductor version 2.8). Expression sets were then filtered according to Calls information. Probe sets expression fold changes between conditions (biological triplicates) were calculated using the "Comparative Marker Selection" module of GenePattern[62]. Volcano and FcFc scatter plots were generated using the Multiplot application of GenePattern. Histogram expression profiles of gene probe sets were generated from MAS values. Further analysis was performed using the Manteia database[63]. Hierarchical clustering was performed on Microarray RMA data. Clustering was computed with an Average linkage method and Euclidean distances. Both an Approximately unbiased (AU) and Bootstrap probability (BP) *P* values were calculated (pvclust, R package). Clusters with AU and BP *P* values > 0.95 are highlighted by color-coded boxes.

Cell preparation and transplantation into tibialis anterior muscles. Serum-free cultures of 3-4 week-old differentiated Pax7-GFP blue mouse ES cells were pretreated with ROCK inhibitor (Y-27632, Tocris), one day before trypsin dissociation. Cell preparation was filtered through 30 µm mesh (Partec) and GFP^+ cells were FACS-sorted. Target cells were resuspended in PBS with tracking fluorescent beads (Molecular probes). 20 µl of cell preparation containing 80,000 to 100,000 cells were injected in the tibialis anterior (TA) muscles of 3- to 4-month-old $Rag1^{-/-}$ Dmd^{mdx_5Cv} male mice ($n = 5$). Injections were done under general anesthesia. Grafted TA muscles were collected 1 to 2 months after transplantation and processed for cryosection and immunohistochemistry. Experiments on mice were done according to local regulations (Boston Children's Hospital, Brigham and Women's Hospital, Institut Pasteur, IGBMC), in agreement with national and international guidelines.

***In situ* hybridization and immunohistochemistry.** Whole mount *in situ* hybridization was carried out as described[64]. Probes for mouse *Msgn1*, *Rspo3*, and *Pax3* were synthesized from mouse embryo cDNA. Probe for *Venus* was synthesized from the Venus plasmid (a kind gift of A. Miyawaki) and probe for *Mesp2* (ref. 65), *Raldh2* (ref. 66) and *Fgf8* (ref. 67) were already described. Images were acquired on a Leica M125 stereomicroscope.

For immunohistochemistry, cell cultures were fixed for 2 h in 4% formaldehyde. Cultures were rinsed three times in PBS, followed by blocking buffer composed of Tris-buffered saline (TBS) supplemented with 1% FBS and 0.1% Triton X-100. Primary antibodies were then diluted in blocking buffer and incubated overnight at 4 °C. Cultures were then washed three times with TBST (TBS supplemented with 0.5% Tween-20) and incubated with secondary antibodies (1:500) and DAPI (5 µg/ml) in blocking buffer for 2 h. Cultures were ultimately washed with TBST followed by PBS, before analysis. Dissected TA muscles were prepared for cryosections (12 µm) as described[68]. Tissue sections were incubated overnight with primary antibodies in blocking buffer. Secondary antibodies conjugated with AlexaFluor (Molecular probes) were used at 1:500 in blocking buffer.

Antibodies used in this study are anti-Tbx6 (a kind gift of Y. Saga[51]), anti-dystrophin (Mandra1, Sigma), anti-dystrophin (Dys1, Leica/Novocastra), anti-Myogenin (Dako, DSHB), anti-Pax3 (DSHB), anti-Pax7 (DSHB), anti-Myod1 (Dako), anti-Laminin (Abcam), anti-Titin (DSHB), anti-GFP (Abcam), anti-Fast MyHC (MY-32, Sigma), anti-MyHC (MF20, DSHB) and anti-Ki67 (Abcam).

Membrane permeability assays. Stage-matched 3- to 4-week-old control and *mdx* ES were cultured as follows. After 4–6 d of culture in RDL medium, cells were changed to a medium supplemented with the FGF inhibitor PD173074 (Sigma) at 250 nM, 0.5% DMSO, and LDN193189 at 0.1 µM. After 2 d of culture in this medium, cells were transferred to a myogenic differentiation medium containing 4 mM L-glutamine, 0.1 mM nonessential amino acids and 2% horse serum (PAA) in DMEM, in which they were maintained for up to 5 weeks. This protocol results in the same myogenic differentiation efficiency as the serum-free protocol described above but leads to less overall cell death resulting in better Evans blue dye staining. Muscle fibers cultures were treated with Evans blue dye (0.2%, Sigma) in N2B27 medium at 37 °C for 45 min. Extra dye was washed away with PBS and cells were reincubated further for 30 min in culture medium, prior to observation. As a permeabilization control, cultures were preincubated with Saponin (Sigma) at 50 µg/ml in culture medium at 4 °C for 20 min prior to staining with Evans blue. Cells were washed with PBS, and cold culture medium was added prior to observation.

Quantifications. *Myofibers density count.* A fiber density estimate was calculated by counting the number of fibers in 3- to 4-week-old control cultures. Quantifications were manually done on an average of 5–10 pictures (at 40–100× magnification) per well, acquired from MyHC-stained myofibers fields. Alternatively, staining was quantified by performing automated cell count using the Array scan XTI (Thermofisher) with a 10× objective (144 fields/well). Image analysis was performed with HCS Studio software. Using the Tube Formation Bioapplication we identified fibers according to myosin staining and measured their area, length and width. Three independent differentiation experiments were quantified. Results are expressed as averages of number of fibers per square millimeter.

Myofibers branching quantification. A branching index was calculated by scoring the number of branches per fiber in 3- to 5-week-old control or *mdx* cultures (two cell lines per genotype). Quantifications were done on an average of 5–10 pictures sets (at 200× magnification) per well, acquired from MyHC and Laminin-stained myofibers fields. Five independent differentiation experiments were scored for branching. A total of 600+ fibers per genotype were scored. Result are expressed in % of fibers.

Myogenic marker quantification. For each marker, immunolabeling was quantified manually on three myogenic fields per well. Alternatively, staining was quantified by performing automated cell count using the Array scan XTI (Thermofisher). Nuclei were segmented using DAPI staining and after a threshold was applied on FITC channel intensity to identify marker-positive cells.

Experiment was performed in triplicate. Result is expressed as a % of positive nuclei.

Image acquisition and processing. Live or fixed brightfield and fluorescent images were acquired either on a Zeiss Axiovert, Evos FL, Zeiss LSM780, or Leica SP5 systems. Images were processed with Adobe Photoshop, and quantification and measurements were done with Fiji[69] software. For muscle contractions, movies were taken with a Leica DMRB microscope using a photometric FX camera and a 20× objective. Images were taken at 100-ms intervals. For movie processing, image sequences were imported and processed in Fiji. Movies were saved in AVI format at a frequency matching the acquisition rate.

Statistical analysis. For array data hierarchical clustering, Approximately unbiased (AU) and BP *P* values were both calculated (pvclust, R package). Clusters with AU and BP $P > 0.95$ were considered significant.

For differential array expression data comparison, unpaired *t*-test *P* values were calculated using the Comparative Marker Selection module of GenePattern[62]. Differences were considered significant for *P* values ≤ 0.05.

For qRT-PCR data, unpaired Student t-test and two-tailed *P* values were calculated. Differences were considered significant for *P* values ≤ 0.05.

For myofibers branching data, statistical analysis was performed using a Fisher's exact test, based on a 2 × 2 contingency table. Differences between groups were considered significant for $P \leq 0.05$.

© 2015 Nature America, Inc. All rights reserved.

52. Nagai, T. *et al.* A variant of yellow fluorescent protein with fast and efficient maturation for cell-biological applications. *Nat. Biotechnol.* **20**, 87–90 (2002).
53. Nagy, A., Rossant, J., Nagy, R., Abramow-Newerly, W. & Roder, J.C. Derivation of completely cell culture-derived mice from early-passage embryonic stem cells. *Proc. Natl. Acad. Sci. USA* **90**, 8424–8428 (1993).
54. Relaix, F. *et al.* The transcriptional activator PAX3-FKHR rescues the defects of Pax3 mutant mice but induces a myogenic gain-of-function phenotype with ligand-independent activation of Met signaling *in vivo*. *Genes Dev.* **17**, 2950–2965 (2003).
55. Kress, C., Vandormael-Pournin, S., Baldacci, P., Cohen-Tannoudji, M. & Babinet, C. Nonpermissiveness for mouse embryonic stem (ES) cell derivation circumvented by a single backcross to 129/Sv strain: establishment of ES cell lines bearing the Omd conditional lethal mutation. *Mamm. Genome* **9**, 998–1001 (1998).
56. Cheng, T.C., Wallace, M.C., Merlie, J.P. & Olson, E.N. Separable regulatory elements governing myogenin transcription in mouse embryogenesis. *Science* **261**, 215–218 (1993).
57. Sambasivan, R. *et al.* Distinct regulatory cascades govern extraocular and pharyngeal arch muscle progenitor cell fates. *Dev. Cell* **16**, 810–821 (2009).
58. Ying, Q.L. *et al.* The ground state of embryonic stem cell self-renewal. *Nature* **453**, 519–523 (2008).
59. Boulting, G.L. *et al.* A functionally characterized test set of human induced pluripotent stem cells. *Nat. Biotechnol.* **29**, 279–286 (2011).
60. Thomson, J.A. *et al.* Embryonic stem cell lines derived from human blastocysts. *Science* **282**, 1145–1147 (1998).
61. Dequéant, M.L. *et al.* A complex oscillating network of signaling genes underlies the mouse segmentation clock. *Science* **314**, 1595–1598 (2006).
62. Reich, M. *et al.* GenePattern 2.0. *Nat. Genet.* **38**, 500–501 (2006).
63. Tassy, O. & Pourquie, O. Manteia, a predictive data mining system for vertebrate genes and its applications to human genetic diseases. *Nucleic Acids Res.* **42** (Database issue), D882–D891 (2014).
64. Henrique, D. *et al.* Expression of a Delta homologue in prospective neurons in the chick. *Nature* **375**, 787–790 (1995).
65. Saga, Y., Hata, N., Koseki, H. & Taketo, M.M. Mesp2: a novel mouse gene expressed in the presegmented mesoderm and essential for segmentation initiation. *Genes Dev.* **11**, 1827–1839 (1997).
66. Niederreither, K., Subbarayan, V., Dolle, P. & Chambon, P. Embryonic retinoic acid synthesis is essential for early mouse post-implantation development. *Nat. Genet.* **21**, 444–448 (1999).
67. Crossley, P.H. & Martin, G.R. The mouse Fgf8 gene encodes a family of polypeptides and is expressed in regions that direct outgrowth and patterning in the developing embryo. *Development* **121**, 439–451 (1995).
68. Mathew, S.J. *et al.* Connective tissue fibroblasts and Tcf4 regulate myogenesis. *Development* **138**, 371–384 (2011).
69. Schindelin, J. *et al.* Fiji: an open-source platform for biological-image analysis. *Nat. Methods* **9**, 676–682 (2012).

© 2015 Nature America, Inc. All rights reserved.

doi:10.1038/nbt.3297